Additional files

Below is the link to the electronic supplementary material.

Additional file 1: Characterization of RTT-hiPSCs. (A) Isogenic RTT-hiPSCs demonstrate similar embryonic stem cell-like morphology and stain positively for the pluripotency markers, NANOG, OCT4, and TRA-1-81. Scale bar for phase contrast images, 500 μm; scale bar for NANOG, OCT4, and TRA-1-81 immunostaining, 50 μm. **(B)** Representative images of teratomas generated in immunodeficient mice that received an intratesticular injection of RTT-hiPSCs. The teratomas corresponded to well-defined, cystic tumors containing tissues of all three germ layers (endoderm, mesoderm, and ectoderm). Scale bar, 100 μm. **(C)** Images of RTT-hiPSC karyotypes. (PDF 246 kb)

Additional file 2: Three-dimensional image of the PCA. The clustering pattern of the cells (hiPSCs vs. neural cells (N) was dependent on the *MECP2* expression pattern and the presence or absence of MeCP2 protein.

Additional file 3: Gene expression analysis of iPSCs. (A) Global gene expression/comparative microarray analyses of undifferentiated hiPSCs and differentiated neural cells. N denotes neural cells. **(B)** Comparison of *NR3C1* gene expression in hiPSCs and differentiated neural cells by qPCR. Relative gene expression was normalized by *ACTB* gene expression. Primer sets are listed in Additional file 5. Data were analyzed by Student's *t*-test and Welch's *t*-test ($*p < 0.05$).

Additional file 4: Properties of neural stem cells derived from RTT-hiPSCs. (A) Diameter (n = 3) and **(B)** number of neurospheres (n = 16) derived from RTT-hiPSCs at 7 days *in vitro*. **(C)** The mRNA expression levels of the neural stem cell markers, *NESTIN* (NES) and *SOX1*, were quantified in RTT hiPSC-derived neurospheres by qPCR. Each value was normalized by comparison with *ACTB* expression and standardized by the value for the wild-type *MECP2*-expressing RS1-52 M clone, which was set to 1 (n = 4). Primer sets are listed in Additional file 5. Data were analyzed by Student's *t*-test and Welch's *t*-test ($*p < 0.05$).

Additional file 5: List of primers used in Additional file 3 and 4.

Authors' contributions

T.A.-N., W.A., Ta.K., and H.O. conceived and designed the experiments and wrote the manuscript. T.A.-N. performed most of the experiments, analyzed the data, and wrote the manuscript. T.A.-N., T.M., Y.O., Te.K., M.O., and H.K. generated the patient-derived hiPSCs and analyzed the culture assay results. R.Y. analyzed the microarray data. T.S. and K.N. performed the bisulfite assay and helped with data analysis. K.M. and T.K. contributed to clinical and genetic analyses of the patient-coordinated study. All the authors read and approved the final version of the manuscript.

Competing interests

H.O. is a scientific consultant for SanBio Co., Ltd. M.S. and A.N. are employed by Takeda Pharmaceutical Co., Ltd. The authors declare that they have no competing interest.

Acknowledgements

We thank the RTT patients and their parents for their cooperation in this study. We also thank J. Kohyama for technical advice on the ChIP assay; M. Isoda, H. Ebise, and H. Nakagawa (Sumitomo Dainippon Pharma Co. Ltd., Osaka, Japan) for help with the microarray analyses; and Y. Imaizumi for expert technical assistance. We also thank all the members of the Okano laboratory for helpful comments and discussions. The research described in this study was partially supported by grants from the New Energy and Industrial Technology Development Organization and the Ministry of Education, Science, Sports and Culture (MEXT) and Ministry of Helath, Labour and Welfare (MHLW) of Japan to H.O.; by the Program for Intractable Disease Research Utilizing Disease-specific iPS Cells funded by the Japan Science and Technology Agency (JST)/Japan Agency for Medical Research and Development (A-MED) to H.O.; by Grants-in-Aid for Scientific Research (KAKENHI); and by the Ministry of Economy, Trade and Industry (METI) of Japan for "Development of Core Technologies for Innovative Drug Development Based Upon IT" in the project focused on developing key technology for discovering and manufacturing drugs for next-generation treatment and diagnosis (the biological-verifying studies) to T.K.

Author details

[1]Division of Medicine and Engineering Science, Interdisciplinary Graduate School of Medicine and Engineering, University of Yamanashi, 4-4-37 Takeda, Yamanashi, Kofu 400-8510, Japan. [2]Department of Physiology, Keio University School of Medicine, 35 Shinanomachi,Shinjuku-ku, Tokyo 160-8582, Japan. [3]Center for Genomic and Regenerative Medicine, Juntendo University School of Medicine, 2-1-1 Hongo, Bunkyo-ku, Tokyo 113-8421, Japan. [4]Department of Epigenetic Medicine, Faculty of Medicine, University of Yamanashi, 1110 Shimokato, Chuo, Yamanashi 409-3898, Japan. [5]Sumitomo Dainipponn Pharma Co. Ltd., Osaka, Osaka 541-0045, Japan. [6]Department of Neurology,School of Meidicine, Aichi Medical University, 1-1 Yazakokarimata, Nagakute, Aichi 480-1195, Japan. [7]Department of Dermatology, Keio University School of Medicine, 35 Shinanomachi,Shinjuku-ku, Tokyo 160-8582, Japan. [8]Department of Stem Cell Biology and Medicine, Graduate School of Medical Sciences, Kyushu University, 3-1-1 Maidashi, Higashi-ku, Fukuoka 812-8582, Japan.

Received: 30 December 2014 Accepted: 30 April 2015
Published online: 27 May 2015

References

1. Fabio RA, Giannatiempo S, Antonietti A, Budden S. The role of stereotypies in overselectivity process in Rett syndrome. Res Dev Disabil. 2009;30:136–45.
2. Hagberg B, Aicardi J, Dias K, Ramos O. A progressive syndrome of autism, dementia, ataxia, and loss of purposeful hand use in girls: Rett's syndrome: report of 35 cases. Ann Neurol. 1983;14:471–9.
3. Bienvenu T, Philippe C, De Roux N, Raynaud M, Bonnefond JP, Pasquier L, et al. The incidence of Rett syndrome in France. Pediatr Neurol. 2006;34:372–5.
4. Webb T, Clarke A, Hanefeld F, Pereira JL, Rosenbloom L, Woods CG. Linkage analysis in Rett syndrome families suggests that there may be a critical region at Xq28. J Med Genet. 1998;35:997–1003.
5. Amir RE, Van den Veyver IB, Wan M, Tran CQ, Francke U, Zoghbi HY. Rett syndrome is caused by mutations in X-linked MECP2, encoding methyl-CpG-binding protein 2. Nat Genet. 1999;23:185–8.
6. Monteggia LM, Kavalali ET. Rett syndrome and the impact of MeCP2 associated transcriptional mechanisms on neurotransmission. Biol Psychiatry. 2009;65:204–10.
7. Ng HH, Zhang Y, Hendrich B, Johnson CA, Turner BM, Erdjument-Bromage H, et al. MBD2 is a transcriptional repressor belonging to the MeCP1 histone deacetylase complex. Nat Genet. 1999;23:58–61.
8. Agarwal N, Becker A, Jost KL, Haase S, Thakur BK, Brero A, et al. MeCP2 Rett mutations affect large scale chromatin organization. Hum Mol Genet. 2011;20:4187–95.
9. Chen WG, Chang Q, Lin Y, Meissner A, West AE, Griffith EC, et al. Derepression of BDNF transcription involves calcium-dependent phosphorylation of MeCP2. Science. 2003;302:885–9.
10. Martinowich K, Hattori D, Wu H, Fouse S, He F, Hu Y, et al. DNA methylation-related chromatin remodeling in activity-dependent BDNF gene regulation. Science. 2003;302:890–3.
11. Horike S, Cai S, Miyano M, Cheng JF, Kohwi-Shigematsu T. Loss of silent-chromatin looping and impaired imprinting of DLX5 in Rett syndrome. Nat Genet. 2005;37:31–40.
12. Chahrour M, Jung SY, Shaw C, Zhou X, Wong ST, Qin J, et al. MeCP2, a key contributor to neurological disease, activates and represses transcription. Science. 2008;320:1224–9.
13. Miyake K, Hirasawa T, Soutome M, Itoh M, Goto Y, Endoh K, et al. The protocadherins, PCDHB1 and PCDH7, are regulated by MeCP2 in neuronal cells and brain tissues: implication for pathogenesis of Rett syndrome. BMC Neurosci. 2011;12:81.
14. Amir RE, Van den Veyver IB, Schultz R, Malicki DM, Tran CQ, Dahle EJ, et al. Influence of mutation type and X chromosome inactivation on Rett syndrome phenotypes. Ann Neurol. 2000;47:670–9.
15. Young JI, Zoghbi HY. X-chromosome inactivation patterns are unbalanced and affect the phenotypic outcome in a mouse model of rett syndrome. Am J Hum Genet. 2004;74:511–20.
16. Gibson JH, Williamson SL, Arbuckle S, Christodoulou J. X chromosome inactivation patterns in brain in Rett syndrome: implications for the disease phenotype. Brain Dev. 2005;27:266–70.

17. Takahashi K, Tanabe K, Ohnuki M, Narita M, Ichisaka T, Tomoda K, et al. Induction of pluripotent stem cells from adult human fibroblasts by defined factors. Cell. 2007;131:861–72.
18. Hotta A, Cheung AY, Farra N, Vijayaragavan K, Seguin CA, Draper JS, et al. Isolation of human iPS cells using EOS lentiviral vectors to select for pluripotency. Nat Methods. 2009;6:370–6.
19. Marchetto MC, Carromeu C, Acab A, Yu D, Yeo GW, Mu Y, et al. A model for neural development and treatment of Rett syndrome using human induced pluripotent stem cells. Cell. 2010;143:527–39.
20. Muotri AR, Marchetto MC, Coufal NG, Oefner R, Yeo G, Nakashima K, et al. L1 retrotransposition in neurons is modulated by MeCP2. Nature. 2010;468:443–6.
21. Cheung AY, Horvath LM, Grafodatskaya D, Pasceri P, Weksberg R, Hotta A, et al. Isolation of MECP2-null Rett Syndrome patient hiPS cells and isogenic controls through X-chromosome inactivation. Hum Mol Genet. 2011;20:2103–15.
22. Kim KY, Hysolli E, Park IH. Neuronal maturation defect in induced pluripotent stem cells from patients with Rett syndrome. Proc Natl Acad Sci U S A. 2011;108:14169–74.
23. Ananiev G, Williams EC, Li H, Chang Q. Isogenic pairs of wild type and mutant induced pluripotent stem cell (iPSC) lines from Rett syndrome patients as in vitro disease model. PLoS One. 2011;6:e25255.
24. Cheung AY, Horvath LM, Carrel L, Ellis J. X-chromosome inactivation in rett syndrome human induced pluripotent stem cells. Front Psychiatry. 2012;3:24.
25. Tanaka Y, Kim KY, Zhong M, Pan X, Weissman SM, Park IH. Transcriptional regulation in pluripotent stem cells by methyl CpG-binding protein 2 (MeCP2). Hum Mol Genet. 2014;23:1045–55.
26. Williams EC, Zhong X, Mohamed A, Li R, Liu Y, Dong Q, Ananiev GE, Mok JC, Lin BR, Lu J, Chiao C, Cherney R, Li H, Zhang SC, Chang Q. Mutant astrocytes differentiated from Rett syndrome patients-specific iPSCs have adverse effects on wild-type neurons. Hum Mol Genet. 2014;23:2968–80.
27. Miyake K, Yang C, Minakuchi Y, Ohori K, Soutome M, Hirasawa T, et al. Comparison of Genomic and Epigenomic Expression in Monozygotic Twins Discordant for Rett Syndrome. PLoS One. 2013;8:e66729.
28. Kubota T, Nonoyama S, Tonoki H, Masuno M, Imaizumi K, Kojima M, et al. A new assay for the analysis of X-chromosome inactivation based on methylation-specific PCR. Hum Genet. 1999;104:49–55.
29. Tchieu J, Kuoy E, Chin MH, Trinh H, Patterson M, Sherman SP, et al. Female human iPSCs retain an inactive X chromosome. Cell Stem Cell. 2010;7:329–42.
30. Ballas N, Lioy DT, Grunseich C, Mandel G. Non-cell autonomous influence of MeCP2-deficient glia on neuronal dendritic morphology. Nat Neurosci. 2009;12:311–7.
31. Skene PJ, Illingworth RS, Webb S, Kerr AR, James KD, Turner DJ, et al. Neuronal MeCP2 is expressed at near histone-octamer levels and globally alters the chromatin state. Mol Cell. 2010;37:457–68.
32. Colantuoni C, Jeon OH, Hyder K, Chenchik A, Khimani AH, Narayanan V, et al. Gene expression profiling in postmortem Rett Syndrome brain: differential gene expression and patient classification. Neurobiol Dis. 2001;8:847–65.
33. Setoguchi H, Namihira M, Kohyama J, Asano H, Sanosaka T, Nakashima K. Methyl-CpG binding proteins are involved in restricting differentiation plasticity in neurons. J Neurosci Res. 2006;84:969–79.
34. Kohyama J, Kojima T, Takatsuka E, Yamashita T, Namiki J, Hsieh J, et al. Epigenetic regulation of neural cell differentiation plasticity in the adult mammalian brain. Proc Natl Acad Sci U S A. 2008;105:18012–7.
35. Okabe Y, Kusaga A, Takahashi T, Mitsumasu C, Murai Y, Tanaka E, et al. Neural development of methyl-CpG-binding protein 2 null embryonic stem cells: a system for studying Rett syndrome. Brain Res. 2010;1360:17–27.
36. Okabe Y, Takahashi T, Mitsumasu C, Kosai K, Tanaka E, Matsuishi T. Alterations of gene expression and glutamate clearance in astrocytes derived from an MeCP2-null mouse model of Rett syndrome. PLoS One. 2012;7:e35354.
37. Tsujimura K, Abematsu M, Kohyama J, Namihira M, Nakashima K. Neuronal differentiation of neural precursor cells is promoted by the methyl-CpG-binding protein MeCP2. Exp Neurol. 2009;219:104–11.
38. Namihira M, Nakashima K, Taga T. Developmental stage dependent regulation of DNA methylation and chromatin modification in a immature astrocyte specific gene promoter. FEBS Lett. 2004;572:184–8.
39. Forbes-Lorman RM, Kurian JR, Auger AP. MeCP2 regulates GFAP expression within the developing brain. Brain Res. 2014;1543:151–8.
40. Ran FA, Hsu PD, Wright J, Agarwala V, Scott DA, Zhang F. Genome engineering using the CRISPR-Cas9 system. Nat Protoc. 2013;8:2281–308.
41. Nagai K, Miyake K, Kubota T. A transcriptional repressor MeCP2 causing Rett syndrome is expressed in embryonic non-neuronal cells and controls their growth. Brain Res Dev Brain Res. 2005;157:103–6.
42. Kishi N, Macklis JD. MeCP2 functions largely cell-autonomously, but also non-cell-autonomously, in neuronal maturation and dendritic arborization of cortical pyramidal neurons. Exp Neurol. 2010;222:51–8.
43. Maezawa I, Swanberg S, Harvey D, LaSalle JM, Jin LW. Rett syndrome astrocytes are abnormal and spread MeCP2 deficiency through gap junctions. J Neurosci. 2009;29:5051–61.
44. Chen RZ, Akbarian S, Tudor M, Jaenisch R. Deficiency of methyl-CpG binding protein-2 in CNS neurons results in a Rett-like phenotype in mice. Nat Genet. 2001;27:327–31.
45. Duncan Armstrong D. Neuropathology of Rett Syndrome. J Child Neurol. 2005;20:747–53.
46. Chahrour M, Zoghbi HY. The story of Rett syndrome: from clinic to neurobiology. Neuron. 2007;56:422–37.
47. Sanacora G, Banasr M. From pathophysiology to novel antidepressant drugs: glial contributions to the pathology and treatment of mood disorders. Biol Psychiatry. 2013;73:1172–9.
48. Czeh B, Di Benedetto B. Antidepressants act directly on astrocytes: evidences and functional consequences. Eur Neuropsychopharmacol. 2013;23:171–85.
49. Ohta S, Imaizumi Y, Okada Y, Akamatsu W, Kuwahara R, Ohyama M, et al. Generation of human melanocytes from induced pluripotent stem cells. PLoS One. 2011;6:e16182.
50. Chaddah R, Arntfield M, Runciman S, Clarke L, van der Kooy D. Clonal neural stem cells from human embryonic stem cell colonies. J Neurosci. 2012;32:7771–81.
51. Eisen MB, Spellman PT, Brown PO, Botstein D. Cluster analysis and display of genome-wide expression patterns. Proc Natl Acad Sci U S A. 1998;95:14863–8.
52. Saeed AI, Sharov V, White J, Li J, Liang W, Bhagabati N, et al. TM4: a free, open-source system for microarray data management and analysis. Biotechniques. 2003;34:374–8.
53. Kimura H, Hayashi-Takanaka Y, Goto Y, Takizawa N, Nozaki N. The organization of histone H3 modifications as revealed by a panel of specific monoclonal antibodies. Cell Struct Funct. 2008;33:61–73.

Akhirin Regulates the Proliferation and Differentiation of Neural Stem Cells in Intact and Injured Mouse Spinal Cord

Felemban Athary Abdulhaleem M,[1,2,3,4] Xiaohong Song,[1,3] Rie Kawano,[1,2] Naohiro Uezono,[5] Ayako Ito,[1] Giasuddin Ahmed,[1] Mahmud Hossain,[1] Kinichi Nakashima,[5] Hideaki Tanaka,[1,2] Kunimasa Ohta[1,2]

[1] Department of Developmental Neurobiology, Graduate School of Medical Sciences, Kumamoto University, Kumamoto 860-8556, Japan

[2] Stem Cell-Based Tissue Regeneration Research and Education Unit, Kumamoto University, Kumamoto 1-1-1 Honjo, Kumamoto 860-8556, Japan

[3] Globle COE "Cell Fate Regulation Research and Education Unit", Kumamoto University, 2-2-1 Honjo, Kumamoto 860-8556, Japan

[4] Ministry of Higher Education- Saudi Arabia, Al Maather Area 225085, Riyadh 11153, Saudi Arabia

[5] Department of Stem Cell Biology and Medicine, Graduate School of Medical Sciences, Kyushu University, Fukuoka 812-8581, Japan

Received 10 July 2014; revised 17 October 2014; accepted 18 October 2014

ABSTRACT: **Although the central nervous system is considered a comparatively static tissue with limited cell turnover, cells with stem cell properties have been isolated from most neural tissues. The spinal cord ependymal cells show neural stem cell potential *in vitro* and *in vivo* in injured spinal cord. However, very little is known regarding the ependymal niche in the mouse spinal cord. We previously reported that a secreted factor, chick Akhirin, is expressed in the ciliary marginal zone of the eye, where it works as a heterophilic cell-adhesion molecule. Here, we describe a new crucial function for mouse Akhirin (M-AKH) in regulating the proliferation and differentiation of progenitors in the mouse spinal cord. During embryonic spinal cord development, M-AKH is transiently expressed in the central canal ependymal cells, which possess latent neural stem cell properties. Targeted inactivation of the AKH gene in mice causes a reduction in the size of the spinal cord and decreases BrdU incorporation in the spinal cord. Remarkably, the expression patterns of ependymal niche molecules in AKH knockout (AKH−/−) mice are different from those of AKH+/+, both *in vitro* and *in vivo*. Furthermore, we provide evidence that AKH expression in the central canal is rapidly upregulated in the injured spinal cord. Taken together, these results indicate that M-AKH plays a crucial role in mouse spinal cord formation by regulating the ependymal niche in the central canal.** © 2014 Wiley Periodicals, Inc. Develop Neurobiol 75: 494–504, 2015

Keywords: **Akhirin; neural stem cells; spinal cord injury; mouse**

Additional Supporting Information may be found in the online version of this article.

Correspondence to: K. Ohta (ohta9203@gpo.kumamoto-u.ac.jp)

Contract grant sponsor: Ministry of Education, Science, Sports, and Culture of Japan (to K.O.).

Contract grant sponsor: Kumamoto University Advanced Research Project "Stem Cell-Based Tissue Regeneration Research and Education Unit" (to A.A.F. and K.O.).

Contract grant sponsor: King Abdullah Scholarship Program (Ministry of Higher Education in Saudi Arabia) (to A.A.F.).

Published online 30 October 2014 in Wiley Online Library (wileyonlinelibrary.com).
DOI 10.1002/dneu.22238

INTRODUCTION

The spinal cord is the caudal portion of the central nervous system (CNS) and transduces the information between the brain and the body. The central canal of the spinal cord is composed of several cell types, which are located either in direct contact with lumen or in a subependymal position. Little is known about the ependymal cell niche of the spinal cord. So far cuboidal, tanycytic, and radial classes of lumen-contacting ciliated ependymal cells, have been identified (Hamilton et al., 2009). Ependymal cells originate from radial glia cells, the neural stem cells in the developing CNS, and they are ciliated cells lining the ventricular walls in the central canal of the spinal cord (Edwards et al., 1990). Numerous studies have shown that only ependymal cells generate progeny of multiple fates, and stem cell activity is included in the ependymal cell population in the intact and damaged spinal cord (Barnabé-Heider et al., 2010). Now, it is widely accepted that the spinal cord ependymal cells show neural stem cell potential both *in vivo* and *in vitro* (Johansson et al., 1999; Namiki and Tator, 1999; Meletis et al., 2008).

Spinal cord injury (SCI) results in rapid and significant loss of mature oligodendrocytes and astrocytes leaving many axons partly denuded (Crowe et al., 1997; Grossman, 2001). As demyelination disturbs the neural circuitry and affects the propagation of action potential, it causes chronic functional impairment. Therefore, rapid remyelination is necessary not only to regain nerve conductance but also to avoid further neurodegeneration. There are two approaches for the use of neural stem cells in the treatment of SCI: (1) transplantation of neural stem cells/progenitors and (2) recruitment of endogenous stem cells. Recent studies have shown that the transplantation of neural stem cells derived from the brains of aborted fetuses, embryonic stem cell-derived neural stem cells, or iPS-derived neural stem cells to the injured spinal cord have a beneficial effect on functional recovery in experimental animals (Okada et al., 2006; Barnabé-Heider and Frisén, 2008; Yasuda et al., 2011; Fujimoto et al., 2012). However, it would be difficult to avoid both the ethical problems of using human fetal tissue and the possibility of immunological rejection by these cell transplantations. Exploring the endogenous spinal cord ependymal cells is another promising approach for cell replacement therapy in SCI. Although the central canal ependymal cells do not display the ability to produce amplifying progenitors under normal conditions, they respond to SCI and start a massive cell division within 24 h (Johansson et al., 1999; Kojima and Tator, 2002; Horky et al., 2006). Then, ependymal cell progeny migrate to the lesion site and differentiate into astrocytes (Frisén et al., 1995; Johansson et al., 1999; Mothe and Tator, 2005; Meletis et al., 2008). However, little is known about the molecular basis of the cellular interactions occurring within the intact and injured spinal cord central canal.

We previously described the isolation of chick-*Akhirin* (C-*AKH*), a soluble molecule displaying high structural homology to vitrin and cochlin consisting of an Limulus factor C, Coch-5b2, and Lgl 1 (LCCL) domain and two von Willebrand factor A (VWA) domains (Ahsan et al., 2005). We showed that C-*AKH* is persistently expressed in the ciliary marginal zone and in lens epithelium cells during chick embryonic eye development. Previous cell adhesion and cell aggregation experiments indicated that *C-AKH* functions as a heterophilic cell-adhesion molecule (Ahsan et al., 2005). Here, we report on novel observations providing evidence that *AKH* controls proliferation and differentiation of progenitors in the mouse spinal cord central canal. We show that *AKH* is transiently expressed in the central canal ependymal cells, which possess latent neural stem cell properties, during the embryonic spinal cord development. In mice lacking the *AKH* gene, we observed a decrease in cell proliferation and an altered cell differentiation in the central canal area. *In vitro* culture assay has shown the reduction of the size, but not the number, of neurospheres derived from *AKH*−/− mice spinal cord. Finally, when the spinal cord is damaged, the expression of *AKH* in the central canal ependymal cells is upregulated. Taken together, these experimental data suggest that *AKH* is involved in the control of spinal cord regeneration as well as embryonic spinal cord formation in mice.

MATERIALS AND METHODS

Mice

AKH null mutant mice were generated by inserting a loxP cassette into the *AKH* coding exon (Supporting Information Fig. S2). All the mice that were used in these studies were backcrossed with the C57BL/6J strain for six generations and can be considered to be of an identical uniform genetic background. All mice experiments were conducted in accordance with guidelines of the Kumamoto University Center for Animal Resources and Development.

Tissue Processing

Mice were deeply anesthetized before transcardial perfusion was performed with phosphate-buffered saline (PBS) and fixed by 4% paraformaldehyde (PFA) in PBS. The

mice spinal cords were harvested and preserved with 20% sucrose overnight at 4°C. The sample was embedded in the optimal cutting temperature (OCT) compound (Tissue TekII, Miles) and was frozen immediately at −80°C. The Frozen transverse serial sections were cut at a thickness of 12–15 μm by cryostat (Leica).

In Situ Hybridization

In situ hybridization (ISH) was performed as previously described (Ahsan et al., 2005) using digoxigenin labeled antisense probe for the *AKH* probe, which were produced from the corresponding DNA construct. Complementary DNAs (cDNAs) for *Nkx2.2*, *Dbx1*, and *Shh* were kindly given to us by K. Shimamura (Kumamoto University, Japan), S. Esumi (Kumamoto University, Japan), and A. Mcmahon (Roche Institute of Molecular Biology), respectively.

Immunohistochemistry

The sections of spinal cord and neurospheres were incubated in PBS containing 5% normal goat serum or 5% skimmed milk for 1 h at room temperature (RT). Sections were incubated overnight at 4°C with the following primary antibodies, Nestin (BD Biosciences), CyclinD2 (Santa Cruz Biotechnology), Vimentin (MILLIPORE), Ki67 (BD Biosciences), Isl1/2 (40.2D), glial fibrillary acidic protein (GFAP; Dako), CD31 (BD Biosciences), Olig2 (MILLIPORE), and Pax6 (MILLIPORE). Then, the sections were washed three times with PBS for 10 min each. Sections were incubated with secondary antibodies for 1 h at RT followed by PBS wash, three times for 10 min each. To visualize the nucleus, Hoechst 3342 (Invitrogen Molecular Probes) was used. Finally, sections were mounted with 90% glycerol and observed under a Nikon Eclipse E600 fluorescence microscope.

Neurosphere Culture

The spinal cords from the early postnatal stage 0 (P0) and 6 (P6) mice were dissected from thoracic region and sliced with a tissue chopper (McILwain). We collected the sliced spinal cord fragments in the culture medium (20 ng/ml epidermal growth factor (EGF), 20 ng/ml fibroblast growth factor (FGF), B27 supplement, 2 m*M* glutamine, and Heparin in Dulbecco Modified Eagle Medium (DMEM) medium) and centrifuged for 5 min. Then, the spinal cord fragments were incubated in 50 μL Trypsin/Ethylenediaminetetraacetic acid (EDTA) (CELL Application) for 3 min at 37°C, and 300 μL of Trypsin Neutralizing Solution (CELL Application) was added and then centrifuged for 2 min. The fragments were dissociated into single cells and they were plated at density of 1×10^4 cells/well in 24-well dishes coated with poly 2-hydroxyethyl methacrylate (0.2 g/ml, SIGMA) at 37°C. The number and the size of neurospheres from P6 spinal cord were examined after 5 days culture. For the neurospheres from P0, secondary spheres were generated from primary spheres after 7 days, and they were processed to immunocytochemistry.

BrdU Labeling

Ten mg/mL of BrdU (SIGMA) was injected into time-pregnant mice at different development stages, and they were sacrificed after 2 h. Spinal cords from the embryos were then harvested and sections were prepared. The slides were preserved with 4 *N* HCl for 30 min at 37°C and washed three times with 0.1 *M* Sodium tetraborate (pH 8.5) and phosphate buffered saline with 0.1% Triton-X-100 (PBST) for 5 min each. Then they were incubated overnight with anti-BrdU antibody (1:300, Abcam) at 4°C. The next day they were washed with PBST three times for 5 min each, the slides were incubated with Cy3-conjugated anti-rat IgG antibody (1:100, Jackson) for 2 h at RT.

SCI Model

We anesthetized C57/BL6 mice (P30, weighing 14–15 g) using a complex mixture of midazolam 4 mg/kg, medetomidine 0.3 mg/kg, and butorphanol 5 mg/kg. This was followed by laminectomies and partial laminectomies at the ninth and tenth thoracic spinal vertebrae, respectively. The dorsal surface of the dura mater was exposed and SCI was induced using an SCI device (50 kdyn; Infinite Horizon impactor, Precision Systems & Instrumentation, Lexington, KY, http://www.presysin.com). The muscle and skin were closed in layers. The mice underwent manual bladder evacuation once a day. The mice were anesthetized and subjected to transcardial perfusion with PBS, followed by 4% PFA in 0.1 *M* PBS pH 7.4, at 1, 3, and 7 days of postinjury. The spinal cords were dissected and fixed in the same fixative at 4°C.

Statistical Analysis

Three pairs of *AKH*+/+ and *AKH*−/− (littermates) mice from their developmental and adult stages were used for *in vivo* studies. For the BrdU and Isl1/2-positive cells at least four sections were counted per embryo at E13.5 and E16.5. The length and width of the neural tube were measured at least for four sections per embryo at E16.5. Neurospheres were counted and the diameter was measured at P6. The mean standard deviation (SD) for all data was calculated. Statistical analysis was performed using Student's *t*-test.

RESULTS

Expression Pattern of *AKH* in the Developing Mouse and Chick Spinal Cord

To assess whether *AKH* is expressed in the mouse spinal cord during the developmental stages, ISH was performed at embryonic Day 9.5 (E9.5), E13.5,

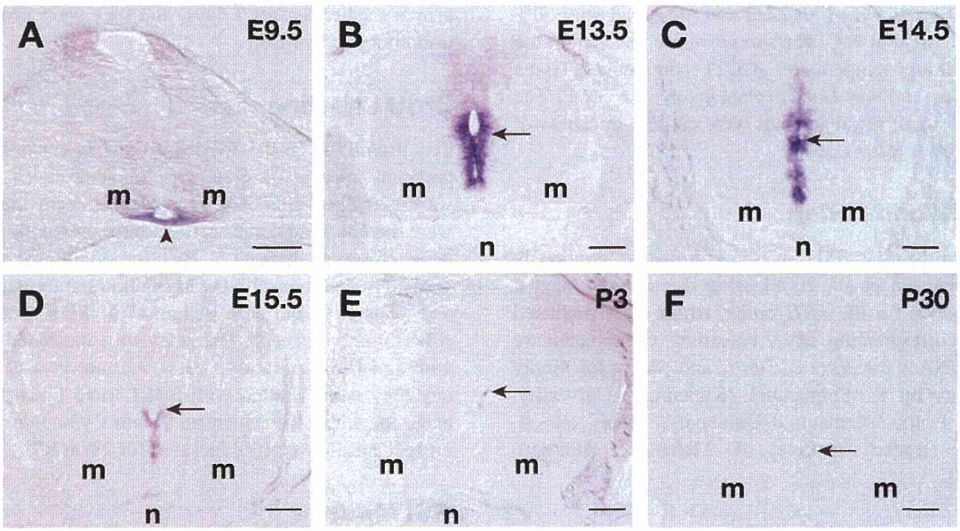

Figure 1 Expression of *AKH* in mouse spinal cord. (A–F): ISH of mouse spinal cord at stage E9.5 (A), E13.5 (B), E14.5 (C), E15.5 (D), P3 (E), and P30 (F). Note that *AKH* expression was first observed in the floor plate (arrowhead) and shifted to the central canal area (arrows) during development. m, motor neuron; n, notochord. Bars: 100 μm. [Color figure can be viewed in the online issue, which is available at wileyonlinelibrary.com.]

E14.5, E15.5, postnatal Day 3 (P3), and adult, respectively [Fig. 1(A–F)]. The earliest expression of *AKH* was observed in the floor plate at E9.5 [Fig. 1(A)] and around the central canal of the neural tube from E13.5 [Fig. 1(B)]. Interestingly, the signal was restricted around the central canal up until the postnatal stage where the location was known to contain neural stem cells. The signal intensity reached its peak at E13.5 and became weaker subsequently [Fig. 1(B–F)]. At E15.5, the *AKH* expression was restricted to the ventral midline region [Fig. 1(D)]. We also examined the C-*AKH* expression during development and found that C-*AKH* was also expressed in the chick spinal cord around the central canal [Supporting Information Fig. S1]. These observations suggest that *AKH* might have a role in stem cell regulation in the spinal cord.

Generation and Phenotype Analyses of *AKH* Deficient Mice

To address the unique role of *AKH* in the mouse spinal cord, *AKH* knockout mice (*AKH*−/−) was generated by replacing the exon with a loxP cassette [Supporting Information Fig. S2]. The homozygous *AKH*−/− mice were viable and fertile. Polymerase chain reaction (PCR) genotyping analysis [Supporting Information Fig. S3(A)] and ISH were performed at E13.5, and on neurospheres, to reveal target mutant mice [Supporting Information Fig. S3(B–E)]. The spinal cord morphology of *AKH*−/− was first examined using Hoechst 3342 at E16.5 [Fig. 2(A, B)]. After measuring the width and length of the neural tube at the thoracic level of *AKH*−/− and *AKH*+/+ mice embryos, we next compared the size difference of the spinal cord between them and found that the size of the neural tube was significantly reduced in the *AKH*−/− mice [Fig. 2(C), Student's *t*-test; $p < 0.05$; Fig. 2(D), Student's *t*-test; $p < 0.01$]. The motoneurons and interneurons in the ventral neural tube are derived from distinct ventricular zone (VZ) progenitor cell population. Each progenitor cell population is defined by an expression pattern of homeodomain neural progenitor genes. Nk2 transcription factor related locus 2 (*Nkx2.2*) was expressed in the neuronal progenitor domain p3 [Supporting Information Fig. S4(D,H)] (Fu et al., 2002), and Developing brain homeobox 1 (*Dbx1*), was expressed in the neuronal progenitor domain p0 [Supporting Information Fig. S4(C,G)] (Kinameri et al., 2008). Moreover, Oligodendrocyte transcription factor 2 (*Olig2*), which expressing motoneuron progenitor (pMN) was examined [Supporting Information Fig. S5(A–F)] (Fu et al., 2002). We compared the expression pattern of these different genes in *AKH*+/+ and *AKH*−/− at the thoracic level. We observed that the defect was not associated with the loss or disorganization of distinct domain and was similar in density and

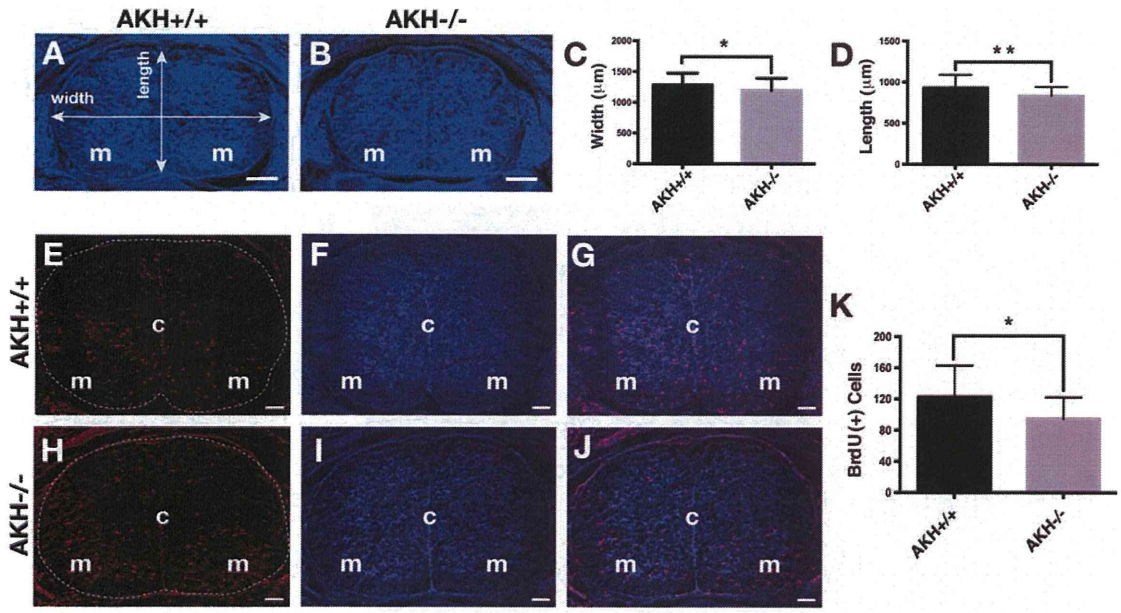

Figure 2 Spinal cord morphology at thoracic level. (A–D): Measurement of the spinal cord size of *AKH*+/+ (A) and *AKH*−/− (B) mice at E16.5. (A, B) Hoechst staining. (C, D) Spinal cord size in width (C) and length (D). Average and SD from four animals are shown. $*p < 0.05$ vs. control; $**p < 0.01$ vs. control; Student's *t*-test. (E–J): Pregnant female mice at E16.5 were injected with a single dose of BrdU and were sacrificed 2 h later. BrdU-labeled cells in *AKH*+/+ (E-G) and *AKH*−/− (H-J) mice spinal cord were counted from four different animals. Bars show the mean number of BrdU-labeled cells in the spinal cord per one section ± SD, calculated from four animals. (K): Quantification of BrdU incorporation in *AKH*+/+ and *AKH*−/− mice spinal cord. $*p < 0.05$ vs. control; Student's *t*-test. m, motoneuron, c, central canal. Bars: 100 μm. [Color figure can be viewed in the online issue, which is available at wileyonlinelibrary.com.]

distribution within *AKH*+/+ and *AKH*−/− mutant mice at E12.5. Likewise, in the floor plate there was no difference in Sonic hedgehog (*Shh*) expression pattern between *AKH*+/+ and *AKH*−/− [Supporting Information Fig. S4(B,F)].

To investigate the effect of the loss of *AKH* on the neural tube, the cell proliferation was analyzed in *AKH*+/+ and *AKH*−/− mice, by subcuteneous administration of 5-bromo-2-deoxyuridine (BrdU), which incorporates into the DNA of cells undergoing S-phase, in time-pregnant mice at E13.5 [Supporting Information Fig. S6] and E16.5 [Fig. 2(E–J)]. We found that BrdU-positive cells were significantly reduced in *AKH*−/− at E13.5 [Supporting Information Fig. S6, Student's *t*-test; $p < 0.01$]. These BrdU-positive cells in *AKH*−/− mice were also decreased in the neural tube compared with *AKH*+/+ at E16.5 [Fig. 2(E,H,K), Student's *t*-test; $p < 0.05$]. Together, this comparison revealed that *AKH* might have some roles in regulating the cell proliferation in the mouse spinal cord.

Loss-of-Function of *AKH* has an Effect on Patterning of the Neural Tube

To illustrate the impact of the loss-of-function of *AKH* during the spinal cord development, we examined whether *AKH* is required to regulate the progenitor cells in the neural tube by immunohistochemical analysis using antibodies against Nestin (neural stem/progenitor cells), GFAP (neural stem cells) in *AKH*−/− and *AKH*+/+ mice at E13.5. The Nestin expression in the central canal of the spinal cords was stronger in the *AKH*+/+ than in *AKH*−/− mice [Fig. 3(A,B)]. Moreover, compared to the *AKH*+/+ the distribution for GFAP in *AKH*−/− mice was also remarkably reduced [Fig. 3(C,D)]. This data indicates that the AKH have role in the regulation of progenitor cells in the spinal cord.

Next, we performed immunohistochemistry using anti-Isl1/2 transcription factor antibody which is expressed in the motoneurons and neurons of the intermediolateral nucleus (Ericson et al., 1992;

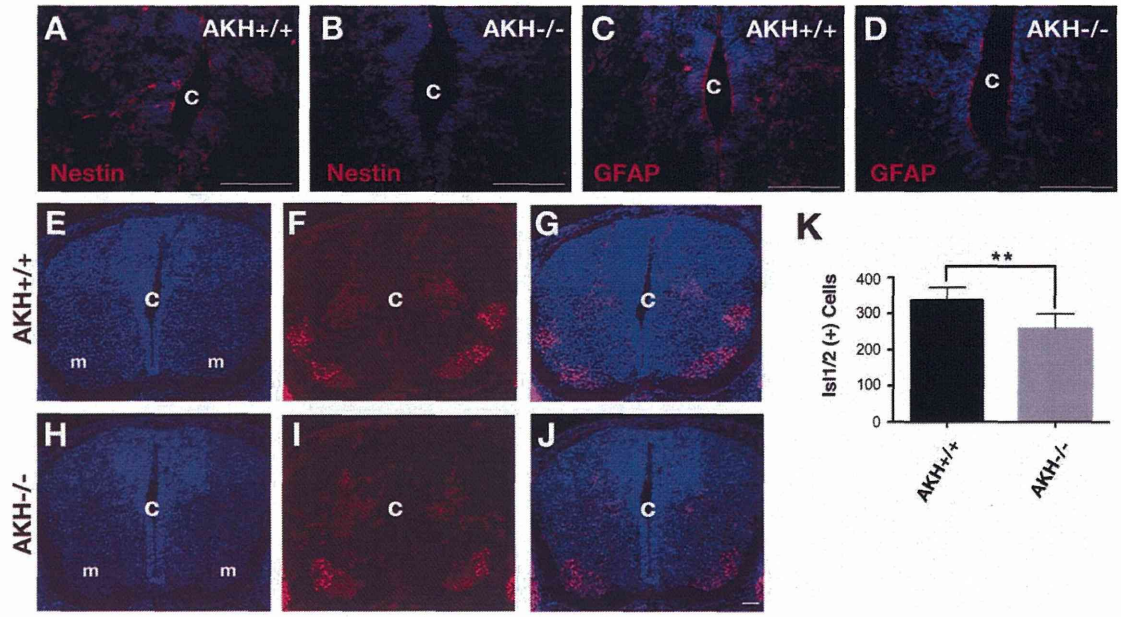

Figure 3 Expression of molecular markers in the spinal cord. (A, B): The immunostaining of *AKH+/+* (A) or *AKH−/−* (B) spinal cord was performed using anti-Nestin antibody at E13.5. (C, D): The immunostaining of *AKH+/+* (C) or *AKH−/−* (D) spinal cord was performed using anti-GFAP antibody at E13.5. (E–J): *AKH+/+* (E–G) and *AKH−/−* (H–J). Hoechst staining (E, H). The immunostaining using anti-Isl1/2 antibody at E13.5 (F, I). Merge (G, J). (K): Quantification of Isl1/2 positive cells in *AKH+/+* and *AKH−/−* mice spinal cord. Average and SD from four animals are shown. $^{**}p < 0.01$ vs. control; Student's *t*-test. c, central canal. m, motoneuron. Bars: 100 μm. [Color figure can be viewed in the online issue, which is available at wileyonlinelibrary.com.]

Tanabe and Jessell, 1996; Liang et al., 2011) and homeodomain neural progenitor gene Pax6. Pax6 is expressed at high levels in the central region of the spinal cord (Goulding et al., 1993). At E13.5, it was observed that the distribution of Isl1/2 protein was reduced in *AKH−/−* relative to wild type littermates [Fig. 3(E–J)]. Quantification revealed that Isl1/2 positive neuron cells were significantly decreased in *AKH−/−* mice [Fig. 3(K), Student's *t*-test; $p < 0.01$]. Additionally, the Pax6 expression was reduced in the central region in p0–p2 [Fig. 4(A–D)] and high magnification [Fig. 4(A',D')] *AKH−/−* compared with *AKH+/+* at E12.5 [Fig. 4(A–F)]. Together, these results demonstrate that *AKH* regulates the cell differentiation for motor neuron and interneuron.

Because the central canal region is surrounded by abundant vasculature, and cellular proliferation within the niche occurs in close proximity to the blood vessels (Hamilton et al., 2009), we assessed whether the blood formation is affected in *AKH−/−* spinal cord at E13.5 using anti-CD31 antibody, which recognizes the endothelial cells. This analysis failed to provide evidence for the involvement of *AKH* in blood vessel formation [Supporting Information Fig. S7].

AKH Affects the Neurosphere Formation in Mouse Spinal Cord

To test the possibility that AKH is involved in the neural stem cell regulation, the neurosphere assay was performed on *AKH−/−* and *AKH+/+* littermate mice at P6. After spinal cord dissection from *AKH−/−* or *AKH+/+* mice, single cells were incubated in 24-well dishes at density 1×10^4 cells/well. We found that the size of the neurospheres in *AKH−/−* mice was significantly reduced compared to control *AKH+/+* mice [Fig. 5(A–C), Student's *t*-test; $p < 0.01$], although no significant difference in the total number of neurospheres was observed between *AKH−/−* and *AKH+/+* [data not shown]. These neurospheres could be cultured for at least seven passages [data not shown]. Through *in vivo* or *in vitro* experiments, this data shows evidence that the neural tube in *AKH−/−* mice and the

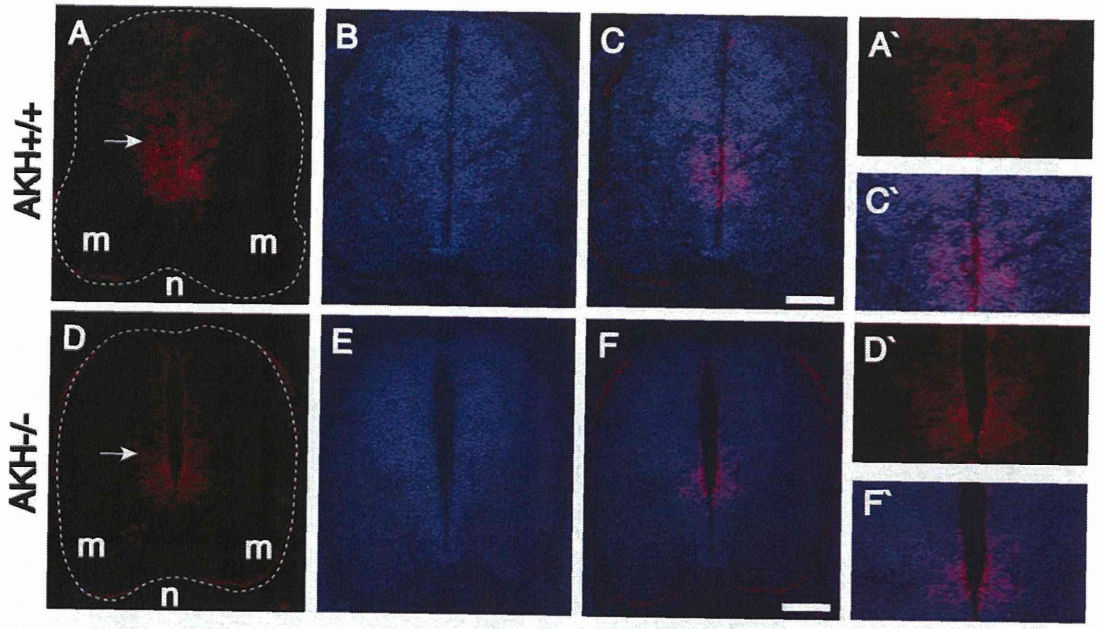

Figure 4 Expression of Pax6 in the spinal cord. (A–F'): The immunostaining of *AKH*+/+ (A) or *AKH*−/− (D) at the thoracic region in the spinal cord was performed using anti-Pax6 antibody at E12.5. Hoechst staining (B, E). Merge (C, F), and high magnification of central region (p0–p2) in the spinal cord (A',C',D', F'). n, notochord. m, motoneuron. Bars: 100 μm. [Color figure can be viewed in the online issue, which is available at wileyonlinelibrary.com.]

neurospheres from it are smaller than that in *AKH*+/+. Because of this, we found that the cell proliferation is limited in *AKH*−/−. Next, we dissected the spinal cords from *AKH*−/− or *AKH*+/+ mice at P0 and cultured them for 7 days. We collected the primary neurospheres and passaged them into secondary neurospheres. Then, we analyzed the expression of different markers in secondary neurospheres by immunocytochemistry [Fig. 5(D–K)]. Triple-immunostaining using Cyclin D2 (Lukaszewicz and Anderson, 2011), Vimentin (the ependymal cell) (Bodega et al., 1994), and Ki67 (the proliferating cell) (Gerdes et al., 1983) antibodies were performed with *AKH*−/− and *AKH*+/+ neurospheres. We observed that Cyclin D2 and Ki67 were expressed in the outer circumference of the neurospheres in the *AKH*+/+ [Fig. 5(D,F)]. In contrast, in *AKH*−/− neurosphere the Cyclin D2 and Ki67 expression was observed throughout the neurospheres area [Fig. 5(H,J)]. Conversely, in both *AKH*−/− and *AKH*+/+ neurospheres, similar immunoreactivity of Vimentin was observed throughout the neurospheres area [Fig. 5(E,I)]. Taken together, this comparison revealed that the distribution of ependymal proliferation and differentiation markers was altered in the neurospheres generated from *AKH*−/− mice spinal cord compared with *AKH*+/+ neurospheres.

AKH Expression is Upregulated After SCI

Several lines of evidence suggest that the ependymal cell niche have a potential for stem cell activity. Moreover, the activity of ependymal cells is rapidly increased after a SCI (Hamilton et al., 2009). As shown in Figure 1F, the expression of *AKH* at P30 spinal cord is very faint or not observed around the central canal of the neural tube. Therefore, we assessed the expression pattern of *AKH* and neural stem/progenitor cell around the central canal after SCI. First, we analyzed whether our manipulation affects the ependymal cells and neural stem cells markers using Nestin and Vimentin antibodies, respectively [Supporting Information Fig. S8(A,B)]. We found that the Nestin- and Vimentin-immunoreactivities were highly upregulated in the injured spinal cord compared to adjacent control segment [Supporting Information Fig. S8(A, B)], indicating that the damaged spinal cord was generated properly. Next, we characterized the expression pattern of *AKH* in the injured spinal cord of P30 *AKH*+/+ mice and compared that to the uninjured adjacent section, on day 1 [Fig. 6(A,B)] and day 7 [Fig. 6(C,D)] after injury. We observed the signal of *AKH* around the central canal, which was upregulated after one and seven days of postinjury [Fig. 6(B,D)]. Thus,

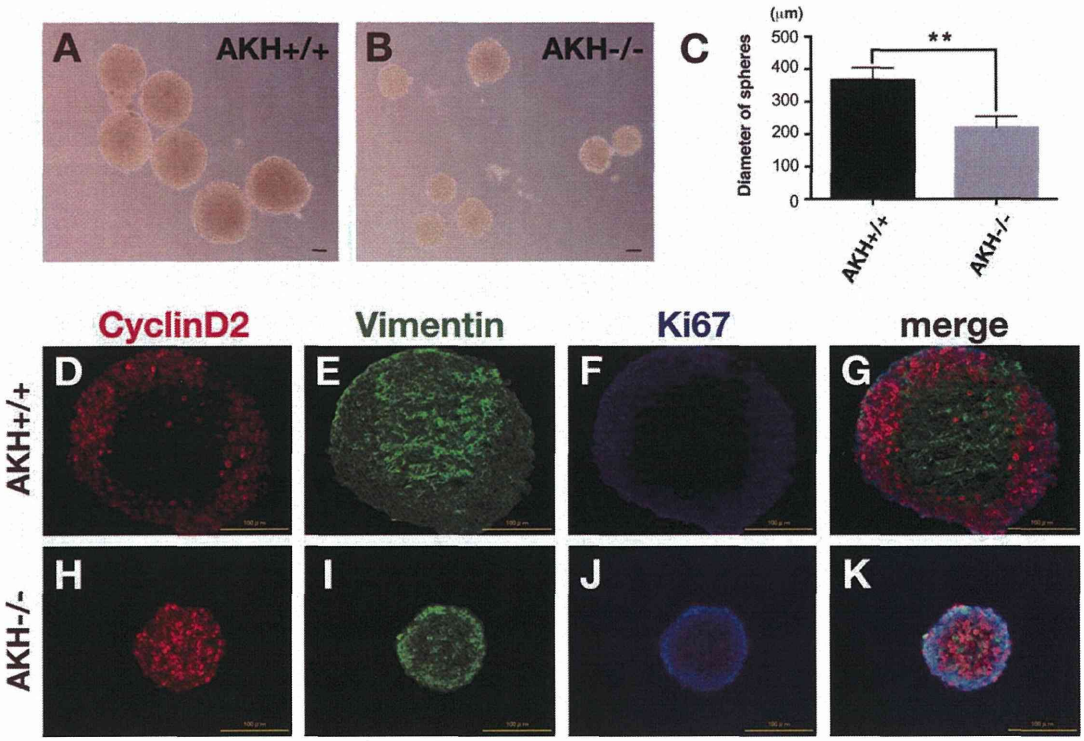

Figure 5 *AKH* affects cell proliferation and differentiation. (A-C): Spheres from *AKH*+/+ (A) or *AKH*−/− (B) spinal cords after 5 days culture. $^{**}p < 0.01$ vs. control; Student's *t*-test. (C) Diameter of neurospheres from *AKH*+/+ and *AKH*−/− mice spinal cord. (D–K): Expression of CyclinD2 (D, H), Vimentin (E, I), Ki67 (F, J), and their merge (G, K) in the spheres derived from *AKH*+/+ (D–G) or *AKH*−/− (H–K). Bars: 100 μm. [Color figure can be viewed in the online issue, which is available at wileyonlinelibrary.com.]

these results suggested that *AKH* might play an important role in the mouse spinal cord after an injury.

To determine the cell-type expressing *AKH* in the ependymal zone of the injured spinal cord at P30 in *AKH*+/+ mice, we performed ISH using *AKH* probe and immunohistochemistry using anti-Vimentin antibody with adjacent sections on day 3 of postinjury [Fig. 6(E–G)]. We found that the Vimentin-positive ependymal cells [Fig. 6(F)] were overlapped with *AKH* expressing cells [Fig. 6(E)] in the central canal [Fig. 6(G)].

DISCUSSION

AKH is Expressed Around Central Canal Region in Mouse and Chick Spinal Cord

The pattern formation and cell fate specification are directed by signaling centers that provide spatial information through the localized production and secretion of protein morphogens. Our observation that *AKH* gradually appeared specifying the location around the central canal of the neural tube in the mouse and chicken spinal cord made us question whether AKH plays an important role around the central canal of the spinal cord during the embryonic stage. Neural stem cells have been isolated from the ependymal zone surrounding the central canal of the spinal cord (Weiss et al., 1996). A recent study demonstrated that neural stem cells are the most dorsally located GFAP-positive cells lying ependymally (Sabourin et al., 2009). As AKH is a soluble molecule expressed in the ependymal cells, it might enhance the stem cell proliferation and differentiation during development. Because several genes involved in Notch, WNT, bone morphogenetic protein (BMP), Hedgehog signaling pathways are expressed in the central canal region (Hugnot, 2010; Hugnot and Franzen, 2011), it will be necessary to identify the AKH partner molecule as AKH functions heterophilically (Ahsan et al., 2005).